Spin–orbit state-selected reactions of Xe$^+$($^2P_{3/2}$ and $^2P_{1/2}$) with H$_2$, D$_2$, and HD

Kent M. Ervin[a]

Department of Chemistry, University of California, Berkeley, California 94720

P. B. Armentrout[b]

Department of Chemistry, University of Utah, Salt Lake City, Utah 84112

Spin–orbit state-selected reactions of Xe$^+$(^2P_J), $J = 3/2$ and $1/2$, with isotopic molecular hydrogen (H$_2$, D$_2$, and HD) to form XeH$^+$ and XeD$^+$ are studied using guided ion beam mass spectrometry. Reaction cross sections are determined as a function of reactant kinetic energy from near thermal energy to 15 eV c.m. Although the reaction of Xe$^+$($^2P_{1/2}$) + H$_2$ to form ground state products XeH$^+$ + H is exothermic, no reaction is observed at low energies and the reaction cross section is zero or small at higher energies. The Xe$^+$($^2P_{3/2}$) + H$_2$ reaction has an apparent threshold near its endothermicity, but the cross section rises slowly above this threshold. The reaction energetics and isotope effects indicate two separate mechanisms for Xe$^+$($^2P_{3/2}$). The dominant mechanism is a direct, impulsive process with an apparent activation barrier. The second mechanism allows reaction near the thermochemical threshold and involves more interaction among all three atoms. These results are interpreted in relation to the spin–orbit coupled potential energy surfaces of XeH$_2^+$ system.

I. INTRODUCTION

In a series of experimental investigations,[1-3] we have studied the hydrogen atom transfer reactions of the rare gas ions with molecular hydrogen,

$$Rg^+ + H_2 \rightarrow RgH^+ + H, \tag{1}$$

where Rg represents He, Ne, Ar, or Kr. This paper completes the series of stable rare gas ions with an examination of the xenon system.

While the hydrogen abstraction process (1) represents a seemingly simple triatomic reaction system, the reactions actually involve multiple potential energy surfaces and exhibit rather complex behavior. Although the reactions with helium and neon[3,4] are strongly exothermic, they do not proceed at thermal energies and have extremely large activation barriers of 8 and 10 eV, respectively. In contrast, reaction (1) with Rg = Ar was long considered[5] to be a classic example of an exothermic reaction which proceeds at the Langevin–Gioumousis–Stevenson collision rate. However, more precise measurements[1,4] indicate that the thermal reaction actually occurs with an efficiency of only two-thirds. Krypton ions also react[2,4] exothermically, although the efficiency is less.

These features can be explained qualitatively by diabatic electronic state correlations between reactants and products, as originally discussed by Mahan.[6] Since RgH$^+$ (Rg = He, Ne, Ar, Kr) dissociates into Rg + H$^+$, ground state products correlate with the asymptotic Rg–H$_2^+$ charge state of reactants rather than with Rg$^+$–H$_2$. The Rg$^+$ + H$_2$ reac-

tants lead diabatically to excited states of the products. This qualitatively explains the high activation barriers in the helium and neon systems, where the Rg$^+$–H$_2$ surface lies far above the Rg–H$_2^+$ surface. In the case of argon and krypton, on the other hand, the two charge states lie close together in energy and these two surfaces intersect near the H$_2$ equilibrium bond length. This crossing is adiabatically avoided as the reactants approach, such that Rg$^+$ + H$_2$ reactants can lead to ground state products. The efficiency of the reaction is determined to first order by the coupling between the charge state surfaces.[1,2]

Orientational effects also influence the reaction efficiency. The rare gas ion Rg$^+$ [s^{2}p^5] can approach hydrogen with three different orientations of the p orbital with the lone electron: P_z, where it is parallel to the axis of approach; P_x, in the plane defined by the three atoms but perpendicular to the axis of approach; and P_y, perpendicular to the plane.[7,8] These orientations correspond to three separate adiabatic surfaces in the entrance channel of the reaction. Molecular orbital considerations indicate that the least repulsive approach of the reactants is a near-collinear P_z orientation.[2,6] It is also the P_z orientation ($^2A'$ surface in C_s symmetry) that adiabatically correlates with the ground state products in the argon and krypton systems,[1,2,6,8] so P_z is the most reactive orientation. The P_x orientation also forms a $^2A'$ surface and the P_y orientation corresponds to a $^2A''$ surface, both of which lead to excited states of the products. These surfaces can couple to the lower reactive surface via nonadiabatic transitions, which are considerably more efficient for the $^2A'$ surface than for the $^2A''$ surface. The observed reaction efficiencies indicate that this nonadiabatic behavior is more probable in argon, where the two charge states are nearly resonant, than in krypton, where the energy separation is greater.[1,2,7,8]
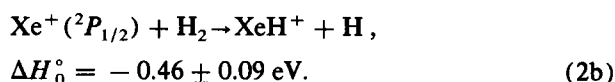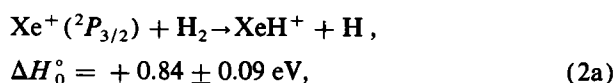
The rare gas ions have two spin–orbit states, the Rg$^+$($^2P_{3/2}$) ground state and the Rg$^+$($^2P_{1/2}$) excited state. Spin–orbit interactions produce mixing of the P_x, P_y, and P_z

"states" described above, and thereby can directly influence the reactivity in these systems. Investigation of spin–orbit effects in chemical reactions is an area of burgeoning interest, recently reviewed by Dagdigian and Campbell.[9] The selection of a particular spin–orbit level of the reactant atom or ion allows one to probe a specific adiabatic potential energy surface of the reaction system. Even in systems with small fine-structure splittings, substantial spin–orbit effects are often found.[9] In systems with large spin–orbit splittings, it might be expected that the higher-energy state would be more reactive, but in fact inverse spin–orbit effects are not uncommon. For example, a strong inverse spin–orbit effect was found in our study of the Kr$^+$ (^2P_J) + H$_2$ reaction.[2] Furthermore, the detailed interpretation of the spin–orbit effects in the krypton system suggested different reactivities not only for the individual states of total angular momentum J in the atomic multiplet, but also a dependence on the m_J component of the angular momentum relative to the line of approach of the reactants.

In this paper, we report the reactions of xenon ions with hydrogen[10–12]:

$$Xe^+ (^2P_{3/2}) + H_2 \rightarrow XeH^+ + H,$$

$$\Delta H_0^\circ = +0.84 \pm 0.09 \text{ eV}, \tag{2a}$$

$$Xe^+ (^2P_{1/2}) + H_2 \rightarrow XeH^+ + H,$$

$$\Delta H_0^\circ = -0.46 \pm 0.09 \text{ eV}. \tag{2b}$$

The xenon system differs from the other Rg$^+$ + H$_2$ systems in several important respects. First, because the ionization potential[12] of xenon, IP(Xe) = 12.130 eV, is lower than that of hydrogen, IP(H) = 13.598 eV, the XeH$^+$ product dissociates adiabatically to Xe$^+$ + H rather than to Rg + H$^+$ as when Rg = He, Ne, Ar, or Kr. As a consequence, the Xe$^+$ + H$_2$ reactants correlate with ground state XeH$^+$ + H and no crossing to the Xe + H$_2^+$ charge-state surface in the entrance channel is required to reach products. Moreover, charge transfer with H$_2$ is endoergic[12] by 3.3 eV for Xe$^+$ ($^2P_{3/2}$) and 2.0 eV for Xe$^+$ ($^2P_{1/2}$), so the Xe + H$_2^+$ surface plays no role at low energies. Second, the spin–orbit splitting in Xe$^+$ is so large (1.31 eV) that little interaction between the Xe$^+$ ($^2P_{3/2}$) + H$_2$ and Xe$^+$ ($^2P_{1/2}$) + H$_2$ potential energy surfaces is expected. Finally, the ground state reaction (2a) is unique among the Rg$^+$ + H$_2$ systems in that it is endothermic. The reaction with Xe$^+$ ($^2P_{1/2}$) is exothermic, but does not occur at thermal energies,[13,14] $k < 10^{-12}$ cm^3 s^{-1}, indicating that there is an activation barrier for reaction (2b). Guided ion beam methods are used here to excite the reactions via translational energy of the reactants. Spin–orbit state-specific reactions[13,14] are employed to produce ion beams of a particular state, as in our study of the analogous reactions of Kr$^+$ (^2P_J).[2] We also investigate the reactions with isotopic hydrogen:

$$Xe^+ (^2P_J) + D_2 \rightarrow XeD^+ + D, \tag{3}$$

$$Xe^+ (^2P_J) + HD \rightarrow XeH^+ + D \tag{4a}$$

$$\rightarrow XeD^+ + H. \tag{4b}$$
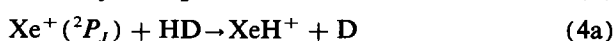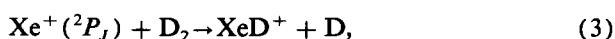
Kinetic isotope effects have proven useful in elucidating the dynamics of hydrogen atom abstraction reactions.[11]

II. EXPERIMENTAL METHODS

The integral cross sections of reactions (2)–(4) are measured from thermal energies up to ion energies of several hundred electron volts using guided ion beam methods. The guided beam apparatus and data analysis procedures have been described in detail elsewhere.[1,15] An outline of the experimental technique is presented here together with a description of the method used to produce spin–orbit state-selected beams of Xe$^+$ (^2P_J) ions.

A. Guided beam cross section measurements

Reactant ions are produced in a drift cell source as described below. The ions are extracted from the ion source, focused into a beam, and mass analyzed in a magnetic sector to select the desired species. The ions are then refocused and injected at the desired ion kinetic energy into a radio-frequency octopole ion beam guide. The octopole creates a radial potential well along the axis of the ion beam which traps ions in radial directions but does not affect their axial velocities. The beam guide passes through a static gas collision cell containing H$_2$, D$_2$, or HD. The octopole trapping field serves to collect scattered product ions efficiently. This greatly improves the sensitivity compared to conventional beam/gas cell instruments and minimizes artifacts due to different collection efficiencies for product ions scattered in different directions.

Neutral reactant densities are kept low enough that multiple ion collisions are improbable. Product ions and unreacted primary ions drift to the end of the octopole, are extracted from it, mass analyzed with a quadrupole mass filter, and detected by secondary electron scintillation and pulse counting electronics. The reaction cross sections are derived directly from the reactant and product ion intensities, the gas cell pressure, and the estimated reaction path length.[1,16] For these experiments, the accuracy of the measured cross sections is limited by the transmission efficiency and mass resolving power of the quadrupole mass analyzer. In particular, a compromise had to be made between transmission efficiency and mass separation for reactions (2) and (4), necessitating rather large Xe$^+$ background subtractions for the XeH$^+$ products. We estimate that the absolute cross sections are within a factor of 2 of the true value and that relative cross section values have an uncertainty of $\pm$ 10% in addition to statistical uncertainties.

The absolute kinetic energy of the ion beam is measured to within $\pm$ 0.1 eV lab by utilizing the octopole itself as a retarding field energy analyzer.[1] Because the energy analysis region and the reaction zone are physically the same, ambiguities in the energy analysis resulting from contact potentials, space charge effects, and focusing aberrations are minimized. Laboratory ion energies are converted to center-of-mass (c.m.) frame energies using the usual stationary target assumption.[1,2]

The initial magnetic mass spectrometer[1] has limited mass resolution and transmits small amounts of xenon isotopes other than the desired one. To avoid problems with isotopic overlap with hydride and deuteride products, the highest-mass xenon isotope, ^{136}Xe(9% natural abundance), is used in all of the experiments reported here. Commercially
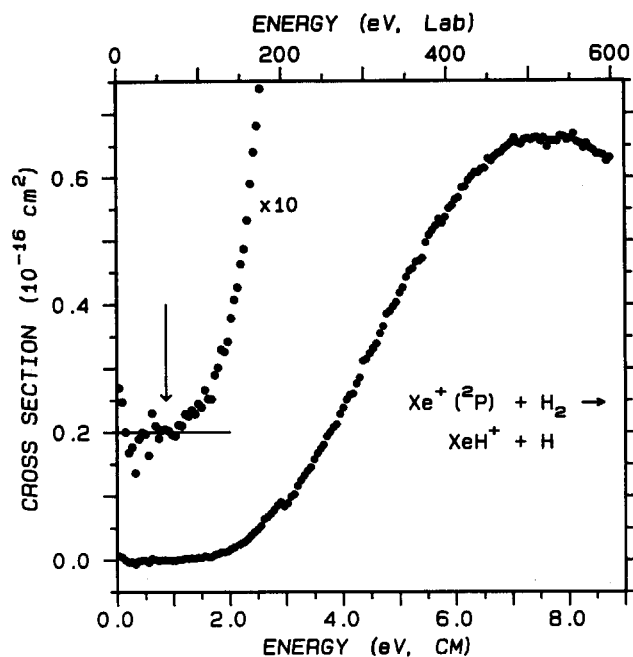
supplied H$_2$ and D$_2$, 99.99%, is used. HD gas has been synthesized by standard methods.[17] According to mass spectrometric and Raman spectroscopic analyses, the HD is at least 98% pure, with approximately equal amounts of H$_2$ and D$_2$ impurities.

B. Xe$^+$ (^2P_J) ion preparation

Xenon ions are prepared using a drift cell ion source which has been described in detail previously.[2,16] Xe$^+$ is initially produced by electron impact ionization. The electron energy is variable and can be kept below the 23.4 eV threshold[18] for formation of metastable excited states above Xe$^+$ (^2P_J). Under similar conditions, Adams et al.[14] found the spin–orbit composition of the ions was near statistical, i.e., ($J = 3/2$):($J = 1/2$) $\approx$ 2:1, and we also obtained a statistical mixture in the case of krypton.[2] These ions are injected into a static gas drift cell, which may be filled with a "filter" gas at a pressure up to 300 mTorr or may remain empty to retain the beam with a mixed spin–orbit state population.

To produce Xe$^+$ ($^2P_{3/2}$) ions, the drift cell is filled with methane, typically to a pressure of 20–30 mTorr. The Xe$^+$ ($^2P_{3/2}$) + CH$_4$ $\rightarrow$ CH$_4^+$ + Xe charge transfer is endothermic and therefore does not occur under the near-thermal conditions of the drift cell, but Xe$^+$ ($^2P_{1/2}$) reacts[14] at a rate of 9.0×10^{-10} cm^3 s^{-1} as follows:

$$\text{Xe}^+(^2P_{1/2}) + \text{CH}_4 \xrightarrow{50\%} \text{CH}_4^+ + \text{Xe}$$

$$\xrightarrow{50\%} \text{Xe}^+(^2P_{3/2}) + \text{CH}_4 .$$

Thus, the Xe$^+$ ($^2P_{1/2}$) state reacts away and the Xe$^+$ ($^2P_{3/2}$) state is enhanced. The actual spin–orbit composition of the ion beam is determined by examining the charge transfer reaction with methane[19] using the usual beam guide techniques (i.e., methane is used both in the drift cell of the ion source to prepare the ions and in the octopole beam guide collision cell to diagnose their spin–orbit populations). Figure 1 shows the methane charge transfer reaction of Xe$^+$ (^2P_J) prepared with and without methane in the drift cell. With no filter gas, there is a strong charge transfer cross section at low energies, indicating that some Xe$^+$ ($^2P_{1/2}$) is present. With methane in the drift cell, the low-energy apparent cross section drops by over two orders of magnitude and a distinct threshold appears. Considering experimental energy broadening, the observed threshold energy corresponds to the 0.47 eV endothermicity for charge transfer with Xe$^+$ ($^2P_{3/2}$). The lack of reaction below the threshold is a clear indication that only Xe$^+$ ($^2P_{3/2}$) is present. Comparison of the charge transfer cross sections for beams made without methane filtering to the rate constant data of Adams et al.[14] verifies our expectation that the composition is near statistical, 29% $\pm$ 5% Xe$^+$ ($^2P_{1/2}$), for electron energies of 20–23 eV in the initial ionization process.

To measure cross sections with a Xe$^+$ (^2P_J) state-selected ion beam, the low-energy reaction of the beam with methane is first monitored while adjusting the drift cell pressure and other source conditions to obtain the desired spin–orbit state composition. The hydrogen reactions are then mea-

FIG. 1. Charge transfer reactions of xenon ions with methane. Cross sections are plotted as a function of the kinetic energy of reactants in the center-of-mass frame (lower x axis) and in the laboratory frame (upper x axis). Crosses show charge transfer for a near-statistical mixture of Xe$^+$ (^2P_J) spin–orbit state, prepared by low-energy electron impact. Circles show data for the Xe$^+$ ($^2P_{3/2}$) ground state, prepared using methane as a filter gas in the drift cell ion source, P (CH$_4$) = 24 mTorr. The cross sections have been corrected for secondary reaction of the charge transfer products.

sured without further changes in ion source conditions, followed by a double check of the spin–orbit state composition using the methane reaction.

We did not find source conditions suitable for making pure Xe$^+$ ($^2P_{1/2}$) ion beams of sufficient intensity for reliable cross section measurements. Candidate filter gases which have larger rate constants[14] with $J = 3/2$ than with $J = 1/2$, such as COS, also depleted the desired $J = 1/2$ state too much, either by reaction or by quenching. Instead, the cross sections for Xe$^+$ ($^2P_{1/2}$) are determined by extrapolation from the measurements with Xe$^+$ ($^2P_{3/2}$) and with statistical mixtures. This procedure is limited in quantitative accuracy because of the uncertainty of the composition of our "statistical" beam and run-to-run deviations in the measured cross sections. To minimize the latter problem, the reactions with pure Xe$^+$ ($^2P_{3/2}$) and with a statistical mixture were performed consecutively with minimal changes in instrumental conditions. Despite large uncertainties in the extrapolated cross section (especially when it is small, as will be found to be the case), the qualitative trends in the reactivity can be determined.

III. RESULTS

A. Xe$^+$(^2P)+H$_2$

The cross section for reaction of a near-statistical mixture of Xe$^+$ (^2P_J) ions with hydrogen is presented in Fig. 2. The cross section has an apparent threshold near 1 eV. The

FIG. 2. Cross section for reaction (2) with a near-statistical mixture of Xe$^+$ (^2P_J) spin–orbit states. The results are plotted as a function of the ion kinetic energy in the laboratory frame (upper scale) and the center-of-mass frame (lower scale). Each point represents an average of several determinations. The inset shows the cross section expanded by a factor of 10 and offset from zero. The arrow indicates the 0.84 eV threshold for reaction of Xe$^+$ ($^2P_{3/2}$).

FIG. 3. Cross sections for reaction (3) with xenon ions prepared with different spin–orbit populations, plotted vs relative kinetic energy (lower scale) and laboratory ion energy (upper scale). Experimental results from a single representative set of measurements are given by circles for ground state Xe$^+$ ($^2P_{3/2}$) and by crosses for a near-statistical mixture of Xe$^+$ (^2P_J). The line gives an extrapolation (assuming a 2:1 mixture of $^2P_{3/2}$:$^2P_{1/2}$ states) of these results to a pure population of the upper spin–orbit state Xe$^+$ ($^2P_{1/2}$).

lack of reaction below this threshold confirms observations[13,14] that Xe$^+$ ($^2P_{1/2}$) does not react at thermal energies, even though reaction (2b) is exothermic.

The ~1 eV apparent threshold corresponds to the endothermicity[12] for reaction (2a), 0.84 ± 0.09 eV, suggesting that Xe$^+$ ($^2P_{3/2}$) is responsible for the observed cross section. The cross section rises very slowly from the apparent threshold until the reaction finally "turns on" at 2.5–3 eV. The slow onset precludes a reliable analysis of the cross section threshold to obtain an independent value of the reaction endothermicity. The cross section peaks in the vicinity of 7.5 eV.

B. Xe$^+$ (^2P_J) + D$_2$

Figure 3 shows the experimental reaction cross sections for reaction (3), both with a statistical mixture of Xe$^+$ (^2P_J) spin–orbit states and with pure Xe$^+$ ($^2P_{3/2}$). The cross section behavior is very similar to reaction (2). When viewed on an expanded scale, the threshold behavior for the statistical mixture is essentially identical to that shown in Fig. 2 for reaction (2). The cross section peaks at 8 eV, then declines monotonically at higher energies.

The Xe$^+$ ($^2P_{3/2}$) + D$_2$ reaction cross section exhibits the same overall behavior as the statistical mixture, but is larger. An extrapolation from the two experimental spin–orbit state populations to pure Xe$^+$ ($^2P_{1/2}$) is also presented in Fig. 3. The scatter in the extrapolated cross section gives an indication of the rather large uncertainty of the extrapolation procedure. The apparently negative cross sections, which are impossible, can be explained by small errors in the

estimated Xe$^+$ (^2P_J) populations in the near-statistical beam or by small relative errors in the cross section magnitudes. Despite these uncertainties, we can make the following conclusions about the spin–orbit state dependence of the reaction. Within experimental error, all of the reactivity of the statistical mixture is accounted for by Xe$^+$ ($^2P_{3/2}$). The experiments do not exclude the possibility of some reaction with Xe$^+$ ($^2P_{1/2}$), but its cross section for reaction is substantially smaller than that for Xe$^+$ ($^2P_{3/2}$).

C. Xe$^+$(^2P_J) + HD

The intramolecular isotope dependence for reaction with HD is shown in Fig. 4. The cross sections for reactions (4a) and (4b) are shown for both a statistical mixture of Xe$^+$ (^2P_J) and for pure Xe$^+$ ($^2P_{3/2}$). The signal-to-noise level in the Xe$^+$ ($^2P_{3/2}$) data is poor because of low beam intensity for the state-selected ions and, for the XeH$^+$ channel, because of the subtraction of background signal from incompletely mass-resolved Xe$^+$. Because of the scatter, we do not attempt a direct extrapolation to the Xe$^+$ ($^2P_{1/2}$) state for these reactions. A heavily smoothed version of the Xe$^+$ ($^2P_{3/2}$) data is provided in Fig. 4 to emphasize the observed structure.

The XeD$^+$ channel, reaction (4b), has an apparent threshold of about 1 eV (same as the reactions with H$_2$ and D$_2$), begins a rapid rise at 1.5 eV (compared to 2.5–3 eV for H$_2$ and D$_2$), and peaks at 5 eV (7–8 eV for H$_2$ and D$_2$). The XeH$^+$ cross section exhibits two features. First, there is a small feature with the same 1 eV apparent threshold as the

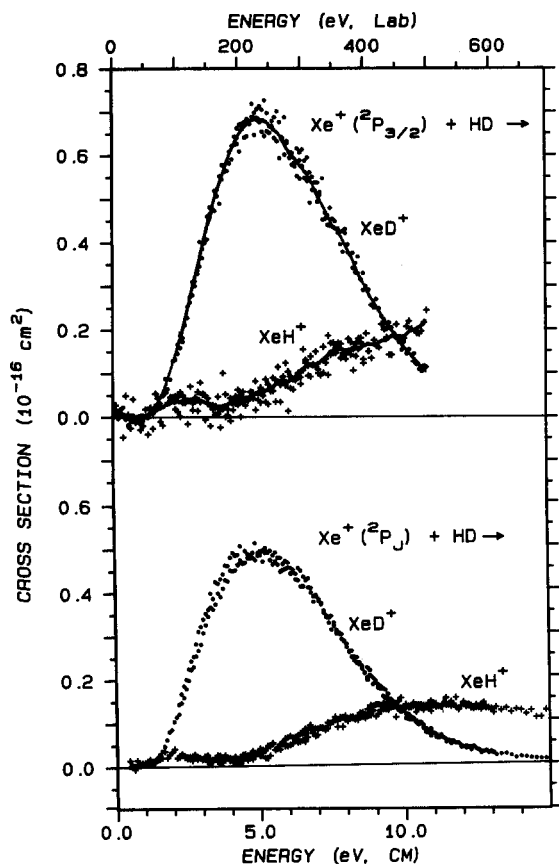FIG. 4. Cross sections for reactions (4a) and (4b) with Xe$^+$ ($^2P_{3/2}$), upper plot, and with a near-statistical mixture of Xe$^+$ (^2P_J), lower plot. A single set of measurements is shown as a function of the reactant kinetic energy in the lab frame (upper axis) and in the center-of-mass frame (lower axis). Small circles indicate the cross sections for formation of XeD$^+$ and crosses indicate the XeH$^+$ product channel. The lines for Xe$^+$ ($^2P_{3/2}$) are heavily smoothed versions of the data, intended to highlight the feature near the threshold for XeH$^+$.

XeD$^+$ channel which peaks at 2–3 eV and then falls off. A second feature rises from approximately 4 eV and extends to higher energies than XeD$^+$ with a broad maximum at 10–12 eV. This unusual behavior is reproducible under different conditions for the statistical mixture of spin–orbit states. It cannot be due to partial mass overlap of the XeH$^+$ and XeD$^+$ products since the minimum in the XeH$^+$ cross section is close to the maximum of the XeD$^+$ cross section.

The XeH$^+$ and XeD$^+$ cross section magnitudes for Xe$^+$ ($^2P_{3/2}$) are $\sim$ 1.5 times that for the statistical mixture of Xe$^+$ (^2P_J). Within experimental error, this is in agreement with a statistical ratio predicted by assuming that the Xe$^+$ ($^2P_{1/2}$) state is nonreactive. Thus, as with reaction (3), the Xe$^+$ ($^2P_{3/2}$) ground spin–orbit state is predominantly responsible for the observed reactivity. In particular, the two XeH$^+$ features persist for pure Xe$^+$ ($^2P_{3/2}$) and hence are not related to different spin–orbit states.

IV. DISCUSSION

There are four prominent features of the XeH$_2^+$ reaction system which we wish to understand: (1) Xe$^+$ ($^2P_{1/2}$) does not react with hydrogen at all at low energies, despite the reaction exothermicity, and its cross section is zero or small at higher energies. (2) The Xe$^+$ ($^2P_{3/2}$) + H$_2$ and Xe$^+$ ($^2P_{3/2}$) + D$_2$ reaction cross sections rise very slowly from their thermochemical thresholds. (3) In the Xe$^+$ ($^2P_{3/2}$) + HD reaction, the XeH$^+$ channel has a curious double maximum with a small feature near threshold and a larger feature at higher energies. (4) The HD reaction exhibits an extremely strong intramolecular isotope effect in which the XeD$^+$ channel dominates at lower energies and rises more rapidly from the thermochemical threshold than in the case of H$_2$ or D$_2$.
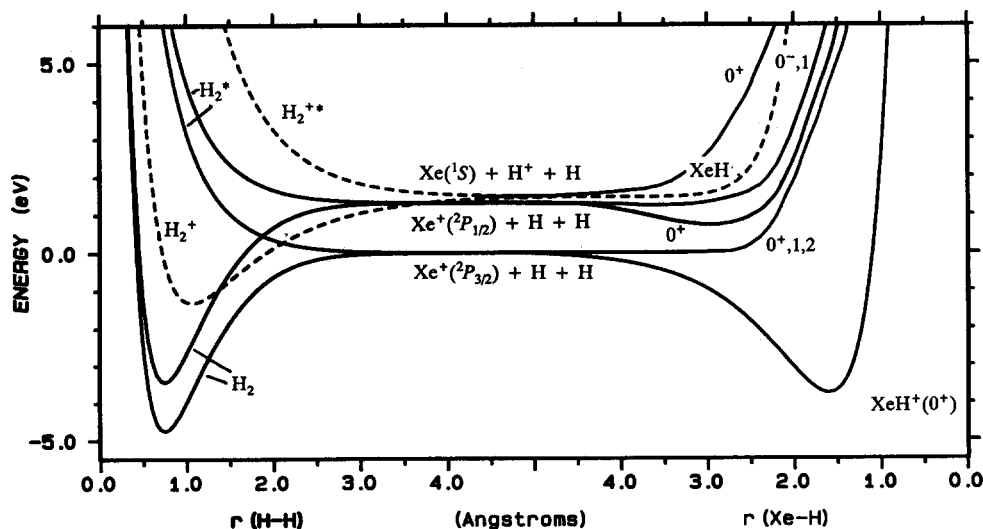
FIG. 5. Schematic asymptotic potential energy curves (Ref. 20) for the XeH$_2^+$ system. The curves on the left represent the potentials as a function of r (H–H) with r (Xe–H) = ∞; the curves on the right represent the potentials as a function of r (Xe–H) with r (H–H) = ∞. The solid lines indicate the potential curves for the diatoms which are a part of reaction (2), H$_2$ and XeH$^+$, while the dashed lines indicate the other charge states, H$_2^+$ and XeH. The notation for designation of the XeH$^+$ states follows Ref. 23.

A. Asymptotic potential energy surfaces

In order to explain these results, we need to examine the potential energy surfaces of the XeH$_2^+$ system. No theoretical information is available about the XeH$_2^+$ intermediate, but correlations between the asymptotic [Xe + H$_2$]$^+$ and [XeH + H]$^+$ states provide a starting point in explaining the reaction dynamics. Figure 5 shows the asymptotic potential energy curves.[20–23] In our work on the other rare gas ions, we treated spin–orbit coupling as a perturbation on the asymptotic potentials, but for Xe$^+$ and XeH$^+$ the spin–orbit splitting is large and must be considered directly. Therefore, the Xe$^+$ ($^2P_{3/2}$) + H$_2$ and Xe$^+$ ($^2P_{1/2}$) + H$_2$ asymptotes are separated in Fig. 5. The valence bond calculations by Gallup,[23] which include spin–orbit coupling empirically, are used for excited XeH$^+$ curves since they dissociate to the correct [Xe + H]$^+$ spin–orbit levels.

Figure 5 shows, as noted in the introduction, that ground state Xe$^+$ + H$_2$ diabatically correlates with ground state XeH$^+$ + H products, i.e., they dissociate to the same atomic asymptote. This contrasts with the other Rg$^+$ + H$_2$ systems, for which the Rg + H$_2^+$ charge state of reactants correlate with ground state RgH$^+$ + H products. For xenon, the Xe + H$_2^+$ curve lies much higher in energy and correlates with repulsive XeH and XeH$^+$ states. Thus, interaction with the charge–transfer surface plays no role in the hydrogen atom transfer reactions of Xe$^+$, at least at low energies.

The spin–orbit coupled potential energy curves indicate that only the Xe$^+$($^2P_{3/2}$) + H$_2$ reactant surface leads to ground state products, while Xe$^+$($^2P_{1/2}$) + H$_2$ correlates with a weakly bound excited state of XeH$^+$.[23] Furthermore, the two sets of curves corresponding to the Xe$^+$($^2P_{3/2}$) and Xe$^+$($^2P_{1/2}$) atomic asymptotes are well separated except for a high-energy crossing of Xe$^+$($^2P_{1/2}$) + H$_2$($^1\Sigma_g^+$) with the repulsive Xe$^+$($^2P_{3/2}$) + H$_2^*$($^3\Sigma_u^+$) surface. These features readily explain the non-reactivity of Xe$^+$($^2P_{1/2}$) with hydrogen: Xe$^+$($^2P_{1/2}$) + H$_2$ leads only to highly excited products, with an endoergicity of about 4 eV. Because of the large energy separation of the two spin–orbit states, there is little probability of nonadiabatic transitions to the lower surface.

B. Reaction energetics and mechanisms

The observation of reaction near the thermochemical threshold, even though the cross sections are small, indicates that there is no potential barrier along the reaction path for the Xe$^+$($^2P_{3/2}$) + H$_2$ surface. Despite this, the reaction mechanism is decidedly nonstatistical as shown by comparison of the experimental cross section with that calculated by using phase space theory.[24,25] This statistical model predicts a much sharper rise from the thermochemical threshold, a larger magnitude for the cross sections [by a factor of 10 at ~4 eV for reactions (2) and (3)], and no dramatic intramolecular isotope effect for reaction (4). We therefore conclude that reactions (2)–(4) are dynamically constrained.

Although the H$_2$ and D$_2$ reactions exhibit some reactivity near the thermochemical threshold, they do not begin to have substantial magnitude until twice that energy. Also, the cross section does not peak until 7–8 eV, much higher than

the 4.5 eV thermodynamic onset for the dissociation process Xe$^+$ + H$_2$ → Xe$^+$ + H + H. Generally, processes where the available energy is distributed among all partners in the reaction are observed to peak at this thermodynamic energy.[11] The delayed onsets and peaks observed in this system are not without precedent, however. Similar behavior has been observed for other systems[26] where the interaction between reactants is repulsive or the reaction is otherwise constrained. Such systems include the rare gas reactions of helium and neon ions with hydrogen[3] and a high-energy feature of the Kr$^+$ ($^2P_{3/2}$) + H$_2$ reaction.[2] The most striking similarity of all these systems is in the HD intramolecular isotope effect: The deuteride product channel is shifted to a lower energy and the hydride channel is shifted to a higher energy compared to the H$_2$ and D$_2$ reactions. Overlooking the threshold feature of reaction (4a) for the moment, this general behavior is also observed for Xe$^+$ ($^2P_{3/2}$) + HD, Fig. 4.

The reaction energetics and isotope effects observed here are characteristic of a direct, impulsive reaction mechanism in which the ion interacts primarily with only one atom in the hydrogen molecule.[26] In this pairwise interaction model, the available energy is not given by the total center-of-mass (c.m.) energy of the ion and the diatom, but rather by the relative energy of the ion and the atom transferred in the reaction. The result in the heavy ion limit[26,27] is that the pairwise interaction energy E_p is one-half the c.m. energy for reactions (2) and (3), one-third for reaction (4a), and two-thirds for reaction (4b). The data for near-statistical Xe$^+$ (^2P_J) in reactions (2)–(4) are plotted on this pairwise energy scale in Fig. 6. Now, the peaks of all the isotopic channels are in the vicinity of 3.5–4.0 eV and the strong onsets are all in the range 0.9–1.4 eV. In particular, the two channels for reactions with HD have similar behavior on the pairwise energy scale, again overlooking the threshold feature in reaction (4a), in contrast to their very different ener-
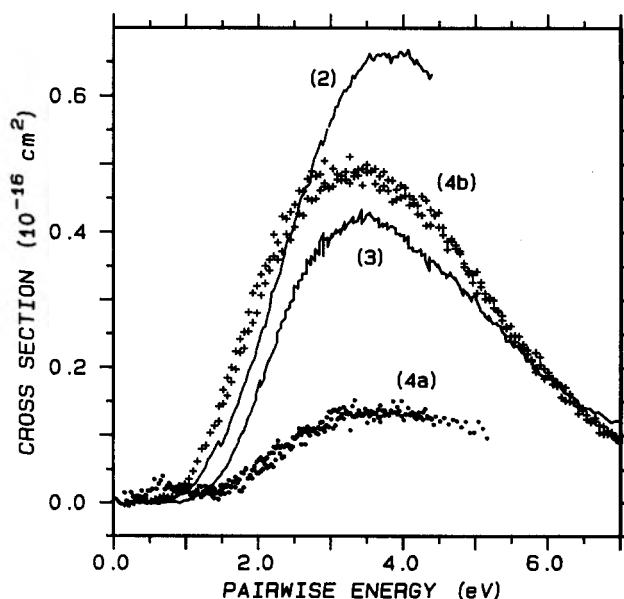

FIG. 6. Cross sections for reactions (2), (3), (4a), and (4b) with near-statistical Xe$^+$ (^2P_J) on the pairwise energy scale, discussed in the text.

getics on the c.m. energy scale, Fig. 4. While the pairwise interaction model is not in detailed quantitative agreement with the isotopic behavior, it does account for the gross features of the dominant reaction mechanism and energetics.

The pairwise energy concept is implicit in the "spectator stripping" kinematic model.[28,29] In spectator stripping, it is further assumed that there is *no* momentum transfer to the third atom, while the more general pairwise interaction model allows a distribution of product energies. Spectator stripping makes a specific prediction for the translational and internal energies of the products: Namely, above the critical pairwise collision energy $E_p = \Delta H_0^\circ + D_0^\circ (RgH^+)$, the diatomic product is internally excited beyond its dissociation energy. Therefore, the atom transfer cross sections would cut off sharply above $E_p \approx 4.5$ eV for the Xe^+ ($^2P_{3/2}$) reactions. It is not surprising that the experimental results, Fig. 6, do not support this prediction since it is unrealistic to restrict the distribution of product energies to the spectator stripping extreme. More realistic models of direct reactions[30] (such as those involving sequential hard sphere collisions) do result in a distribution of product energies. However, they do not reproduce the strong energetic shifts at lower energies, since they give essentially hard sphere cross sections in that regime.

A further observation illustrated by Fig. 6 is that the cross section for reaction (4b) is larger than that of reaction (4a). There are two possible (nonexclusive) explanations for this. The first is simply that the threshold for the XeH^+ channel occurs at higher c.m. energies than that for the XeD^+ channel. Thus, the energetic requirements for the former reaction are more severe resulting in a smaller overall cross section magnitude, independent of the isotopic branching ratio controlled by the pairwise collision kinematics. The second explanation invokes a *collinear* hard sphere collision model, as described by Mahan and co-workers[31] and discussed by Chivalak and Hierl[32] in relation to Kr^+ + HD reaction. In an ideal collinear hard sphere collision, deuteride product formation in the HD reaction requires two sequential binary collisions among the three atoms while hydride product formation requires four collisions, thus making product formation less likely for the latter. While exactly collinear trajectories are improbable, the molecular orbital arguments mentioned in the introduction do favor near-collinear processes for the Rg^+ + H_2 systems.

We shall now consider the threshold feature in reaction (4a). As noted above, the two features of reaction (4a) cannot be attributed to reactions of different spin–orbit states. Instead, we conjecture that the low-energy feature is due to a second reaction mechanism which actually occurs in each of the isotopic reactions. This second mechanism would account for the reactivity near the thermochemical thresholds of reactions (2), (3), and (4b), i.e., below the pairwise energy thresholds. Unfortunately, if a feature with similar behavior and magnitude to that for process (4a) appeared in any of the other reactions, it would be obscured by the dominant feature in the cross section (the pairwise impulsive mechanism). Thus, an obvious low energy feature is observed only for reaction (4a) because there the dominant process is shifted to higher energies according to the pairwise interaction

model described above.

The low-energy mechanism must be one in which all three atoms are involved in a intimate collision, although the mechanism need not involve a long-lived intermediate. For such a process, the c.m. energy is available to promote the reaction. Thus, reaction at the thermodynamic threshold is possible and the XeH^+ and XeD^+ products of reaction (4) should have similar energy dependences. If this is the case, then differentiation of the two mechanisms could be achieved by experiments capable of examining the kinetic energy or angular distributions of the products.

C. Reaction pathways

A closer examination of the ground state potential energy surface can provide some insight into the origins of the two reaction mechanisms. Figure 7 shows the adiabatic electronic state correlation diagram which connects the He^+ (^2P_j) + H_2 reactant states with XeH^+ + H products. The correlations merely indicate which states are connected according to symmetry for (C_s geometries), without any assumptions about the actual nature of the surface along the reaction path. As already determined from the asymptotic potential energy curves, the Xe^+ ($^2P_{1/2}$) + H_2 surface correlates with highly excited products and is therefore unreactive, in agreement with experiment. The Xe^+ ($^2P_{3/2}$) + H_2 has two components: a $^2A'$ surface arises from Xe^+ ($^2P_{3/2}$, $m_J = \pm 1/2$) + H_2 and a $^2A''$ surface arises from Xe^+ ($^2P_{3/2}$, $m_J = \pm 3/2$). Only the $^2A'$ surface adiabatically correlates with ground state products.

The low-energy reaction mechanism which begins near the thermodynamic threshold must proceed along the $^2A'$ potential energy surface. Consequently, there must be little or no barrier to reaction along this surface, and yet the reaction is quite inefficient in the threshold region. This can be understood by using the molecular orbital considerations[6,11] discussed in the introduction. These indicate that the least repulsive approach of Xe^+ (^2P) to H_2 is collinear with the p orbital with the unpaired electron directed along the H–H
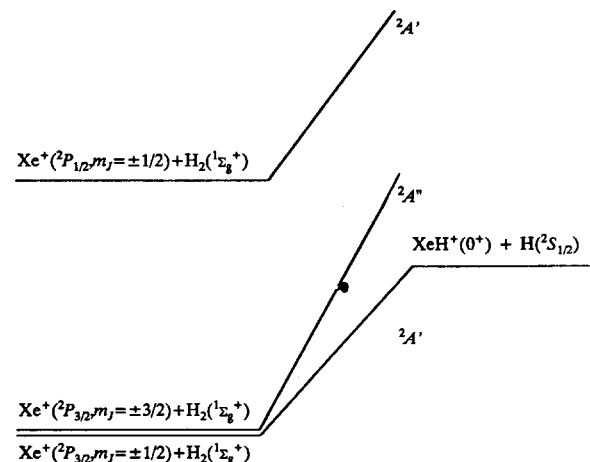

FIG. 7. Partial adiabatic electronic state correlation diagram for reaction (2).

bond. This P_z "state" is the major component[2,11] of the Xe+ ($^2P_{3/2}$, $m_J = \pm 1/2$) state, which corresponds to the ground $^2A'$ surface, Fig. 7. Note, however, that as the Xe+–H–H intermediate deviates from a collinear orientation, the nonbonding doubly occupied p orbitals on Xe+ can begin to interact with the trailing H atom. This interaction is strongly repulsive such that bent geometries are disfavored. The constraint for collinear geometries accounts for the small reaction cross section observed at the thermodynamic threshold. Similar arguments have been advanced to explain comparable behavior in other systems.[11,26]

The dominant reaction mechanism appears to involve a pairwise impulsive interaction. This indicates that reaction occurs along a repulsive potential energy surface. We can imagine two processes which could contribute. The first is simply due to noncollinear orientations along the ground state $^2A'$ reaction surface. The second is analogous to our interpretation for the high-energy feature in the Kr+ ($^2P_{3/2}$) + H_2 reaction, which exhibits strikingly similar magnitudes and energetics to those observed here for Xe+ ($^2P_{3/2}$) + H_2. We suggested that this Kr+ feature was due to nonadiabatic transitions from the $^2A''$ to the $^2A'$ surface. The $^2A''$ surface arises from Rg+ ($^2P_{3/2}$, $m_J = \pm 3/2$) + H_2, has no P_z character,[2] and therefore is expected to be repulsive. Transitions between A'' and A' surfaces are normally forbidden for triatomic systems, but can be induced by electronic–rotational (Coriolis) coupling.[33] Coriolis coupling occurs when high rotational velocities of the collision plane of the reactants—possible at high collision energies and small impact parameters—cause the electrons to "lag" out of the plane. A detailed theoretical examination of these systems would help resolve the relative contributions of reaction along the $^2A'$ and $^2A''$ surfaces and the origins of the two reaction mechanisms.

V. SUMMARY

Spin–orbit state-selected cross sections have been measured for the hydrogen atom transfer reactions of Xe+ (^2P_J) with H_2, D_2, and HD. Selection of particular spin–orbit states of the reactant ions provides probes of different adiabatic reaction surfaces. Kinetic isotope effects are examined to elucidate the reaction dynamics.

Xe+ ($^2P_{1/2}$) does not react with hydrogen, even though formation of ground state XeH+ + H is exothermic, because the $^2A'$ surface which correlates with Xe+ ($^2P_{1/2}$) + H_2 leads to excited product states. Xe+ ($^2P_{3/2}$) reacts via two separate mechanisms. The weaker process is allowed near the thermochemical threshold for the reaction and probably involves intimate interactions among all three atoms of the XeH$_2^+$ system. This must occur along the $^2A'$ surface which adiabatically connects Xe+ ($^2P_{3/2}$, $m_J = \pm 1/2$) + H_2 reactants with ground state products. The dominant mechanism is a direct, impulsive process with an apparent activation barrier in the c.m. energy frame. This mechanism could arise from noncollinear collisions on the ground state $^2A'$ surface or from nonadiabatic transitions from the $^2A''$ surface which emanates from Xe+ ($^2P_{3/2}$, $m_J = \pm 3/2$) + H_2 to the lower $^2A'$ sur-

face. These nonadiabatic transitions may be induced by electronic–rotational (Coriolis) coupling.

[1]K. M. Ervin and P. B. Armentrout, J. Chem. Phys. **83**, 166 (1985).
[2]K. M. Ervin and P. B. Armentrout, J. Chem. Phys. **85**, 6380 (1986).
[3]K. M. Ervin and P. B. Armentrout, J. Chem. Phys. **86**, 6240 (1987).
[4]Please see Refs. 1, 2, and 3 for literature citations on the argon, krypton, and helium/neon systems, respectively.
[5]M. Henchman, in *Ion–Molecule Reactions*, edited by J. L. Franklin (Plenum, New York, 1972), Vol. I, p. 101.
[6]B. H. Mahan, J. Chem. Phys. **55**, 1436 (1971); Acc. Chem. Res. **8**, 55 (1975).
[7]P. J. Kuntz and A. C. Roach, J. Chem. Soc. Faraday Trans. 2 **68**, 259 (1972).
[8]S. Chapman, J. Chem. Phys. **82**, 4033 (1985).
[9]P. J. Dagdigian and M. L. Campbell, Chem. Rev. **87**, 1 (1987).
[10]Preliminary results for this system have been presented previously (Ref. 11).
[11]P. B. Armentrout, in *Structure/Reactivity and Thermochemistry of Ions*, edited by P. Ausloos and S. G. Lias, NATO Adv. Study Inst. Ser., Ser. C: Math. Phys. Sci. (D. Reidel, Dordrecht, Holland, 1987), Vol. 193, pp. 97–164.
[12]Reaction enthalpies are derived from the experimental proton affinity of xenon, PA$_{298}$(Xe) = 118.6 $\pm$ 2 kcal/mol [S. G. Lias, J. Liebman, and R. D. Levin, J. Phys. Chem. Ref. Data **13**, 695 (1984)], corrected to 0 K to yield D_0°(Xe+–H) = 3.64 $\pm$ 0.09 eV; the spectroscopic value for the bond energy of hydrogen D_0°(H_2) = 4.4781 eV [K. P. Huber and G. Herzberg, *Constants of Diatomic Molecules* (Van Nostrand Reinhold, New York, 1979)]; and tabulated ionization potentials [H. M. Rosenstock, K. Draxl, B. W. Steiner, and J. T. Herron, J. Phys. Chem. Ref. Data 6, Suppl. 1 (1977)]. A theoretical value for the XeH+ bond dissociation energy, D_0°(Xe+–H) = 3.90 $\pm$ 0.1 eV [R. Klein and P. Rosmus, Z. Naturforsch. Teil A **39**, 349 (1984)], gives enthalpy values of ΔH_0° = 0.58 $\pm$ 0.1 eV for reaction (2a) and ΔH_0° = – 0.73 $\pm$ 0.1 eV for reaction (2b).
[13]R. D. Smith, D. L. Smith, and J. H. Futrell, Int. J. Mass Spectrom. Ion Phys. **19**, 395 (1976).
[14]N. G. Adams, D. Smith, and E. Alge, J. Phys. B **13**, 3235 (1980).
[15]K. M. Ervin, Ph.D. thesis, University of California, Berkeley, 1986.
[16]K. M. Ervin and P. B. Armentrout, J. Chem. Phys. **84**, 6738 (1986).
[17]I. Wendel, R. A. Friedel, and M. Orchin, J. Am. Chem. Soc. **71**, 1140 (1949).
[18]C. E. Moore, *Atomic Energy Levels*, Nat. Bur. Stand. Circ. **467** (U.S. GPO, Washington, D.C., 1958).
[19]Other product channels, such as formation of XeH+ and XeCH$_3^+$ products [G. D. Miller, L. W. Strattan, C. L. Cole, and P. M. Hierl, J. Chem. Phys. **74**, 5082 (1981); G. D. Miller, L. W. Strattan, and P. M. Hierl, *ibid.* **74**, 5093 (1981)], are relatively minor and do not affect the charge transfer measurements.
[20]The ground and excited state curves of H_2 and H_2^+ are generated from the modified Morse potentials given in Ref. 7. The potential energy curve for ground state XeH+ is a Morse potential based on the experimental vibrational constant (Ref. 22) and bond energy (Ref. 12). The excited XeH+ curves are taken from Ref. 23 and the XeH potential is from Ref. 21.
[21]P. Huxley, D. B. Knowles, J. N. Murrel, and J. D. Watts, J. Chem. Soc. Faraday Trans. 2 **80**, 1349 (1984).
[22]S. A. Rogers, C. R. Brazier, and P. F. Bernath, J. Chem. Phys. **87**, 159 (1987).
[23]G. A. Gallup and J. Macek, J. Phys. B **10**, 1601 (1977).
[24]W. J. Chesnavich and M. T. Bowers, J. Chem. Phys. **66**, 2306 (1977); D. A. Webb and W. J. Chesnavich, J. Phys. Chem. **87**, 3791 (1983).
[25]K. M. Ervin and P. B. Armentrout, J. Chem. Phys. **84**, 6750 (1986).
[26]J. L. Elkind and P. B. Armentrout, J. Chem. Phys. **84**, 4862 (1986); J. Phys. Chem. **90**, 5736 (1986); R. Georgiadis and P. B. Armentrout, *ibid.* (in press).

[27]The exact mass factor is given by Eq. (14) of Ref. 3.

[28]R. D. Levine and R. B. Bernstein, *Molecular Reaction Dynamics and Chemical Reactivity* (Oxford, New York, 1987), pp. 10–13.

[29]A. Henglein, in *Ion–Molecule Reactions in the Gas Phase*, edited by P. J. Ausloos (American Chemical Society, Washington, D.C., 1966), p. 63; A. Henglein and K. Lacmann, Adv. Mass Spectrom. 3, 331 (1966).

[30]For example, T. F. George and R. J. Suplinskas, J. Chem. Phys. 54, 1037, 1046 (1971); B. H. Mahan, W. E. W. Ruska, and J. S. Winn, *ibid.* 65, 3888

(1976); D. A. Micha and J.-M. Yuan, *ibid.* 63, 5462 (1975); J.-M. Yuan and D. A. Micha, *ibid.* 64, 1032 (1976); P. B. Armentrout and J. L. Beauchamp, Chem. Phys. 48, 315 (1980).

[31]K. T. Gillen, B. H. Mahan, and J. S. Winn, J. Chem. Phys. 58, 5373 (1973).

[32]S. Chivalak and P. M. Hierl, Chem. Phys. Lett. 45, 99 (1977); J. Chem. Phys. 67, 4654 (1977).

[33]H. Laue, J. Chem. Phys. 59, 3034 (1967).